Ultraviolet laser-induced submicron spatially resolved superhydrophilicity on single crystal lithium niobate surfaces

A. C. Muir,[a] S. Mailis, and R. W. Eason
Optoelectronics Research Centre, University of Southampton, Hants SO17 1BJ, United Kingdom

(Received 21 February 2007; accepted 29 March 2007; published online 31 May 2007)

Lithium niobate crystal surfaces become superhydrophilic after ultraviolet laser irradiation. The crystal surface hydrophilicity, which was assessed by the contact angle of a sessile drop of de-ionized water, was found to undergo a transition from mildly hydrophobic (contact angle $\theta_E \approx 50°$) to a superhydrophilic state ($\theta_E < 5°$). Patterning of the hydrophilicity at the micron and submicron ranges has been achieved by spatially modulating the illuminating laser beam. © *2007 American Institute of Physics*. [DOI: 10.1063/1.2734539]

I. INTRODUCTION

Lithium niobate (LN) is a material that has found many uses in the optoelectronics industry due to its large electro-optic, acousto-optic, and nonlinear coefficients. In the development of devices which exploit these properties the wettability of the surface is often of great importance either during fabrication[1,2] or as an integral property of the final device.[3] Currently the wetting properties of LN surfaces are altered through the functionalization of the surface with solutions such as $NH_4OH+H_2O_2+H_2O$ (Ref. 1) or by depositing monolayers such as octadecyltrichlorosilane.[3] Structuring of these coatings is currently achieved through the multiple processing steps of photolithography that may disrupt or further complicate the construction of other device components.

In this paper we show that it is possible to achieve a change of the inherent wetting properties of the crystal surface simply by exposing to ultraviolet (UV) irradiation at photon energies exceeding the band gap of the material. It is also shown that the change in wetting behavior can be spatially resolved down to the submicron scale.

II. SESSILE DROP INVESTGATION

A. Experimental details

Experiments characterizing the hydrophilicity change using sessile water drops have been carried out using a range of different lasers [with wavelengths (λ) of 244, 248, and 266 nm] which were either pulsed, with pulse durations ranging from 130 fs to 20 ns, or continuous wave. Ultrafast laser exposures were carried out at λ=266 nm using the third harmonic of a Coherent Mira oscillator–Legend amplifier system. The laser beam (pulse duration of 130 fs, repetition rate of 1 kHz) was expanded to give an energy fluence of 0.045 mJ cm^{-2} per pulse. Nanosecond laser exposures were carried out at λ=266 nm ($Nd:YVO_4$ laser, 20 ns pulse duration, 20 Hz repetition rate) and λ=248 nm (KrF laser, pulse duration of 20 ns, repetition rate of 10 Hz). The λ=266 nm beam was expanded to give an energy fluence of 2 mJ cm^{-2} per pulse and the λ=248 nm beam was truncated by a 6×6 mm^2, square aperture to give an energy fluence at the sample of 40 mJ cm^{-2} per pulse. The exposures using the femtosecond and nanosecond lasers were carried out at ambient laboratory conditions.

The continuous wave exposures were carried out at λ=244 nm using a frequency doubled argon ion laser, and the slightly elliptical beam provided by the laser was expanded to give a spot with a major axis of 12 mm and minor axis of 10 mm. Exposures were carried out over a range of incident powers from 10 to 60 mW in an environmental chamber which provides a controlled environment of pressure, temperature, and atmosphere. Large glass windows enabled optical monitoring of the surface for the contact angle measurements. The UV illumination of the samples was performed through a fused silica window and the exposure time was controlled by a computer controlled shutter. After UV exposure a 0.5 μl drop of de-ionized (DI) water was immediately placed on the surface and the drop profile was imaged and captured using a charge coupled device (CCD) camera. The contact angle was measured using an image analysis software.[4]

B. Results and discussion

Figure 1 shows the effect of UV irradiation upon the contact angle of a sessile drop and defines the contact angle θ_E as the angle between the substrate surface and the tangent to the drop profile at the line where the solid, liquid, and vapor phases meet. The upper picture [Fig. 1(a)] shows a drop of DI water on an unilluminated surface and the lower

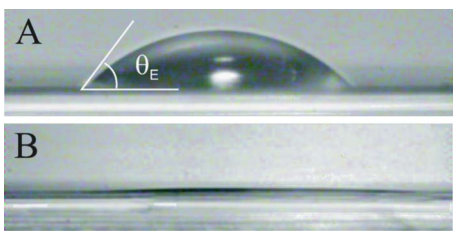

FIG. 1. Effect of the contact angle (θ_E) of a DI water sessile drop on LN after exposure to UV light. (A) shows the contact angle of a drop on an unilluminated surface. (B) shows a drop that has wetted the LN surface after exposure to UV light.

[a]Author to whom correspondence should be addressed; electronic mail: acm@orc.soton.ac.uk

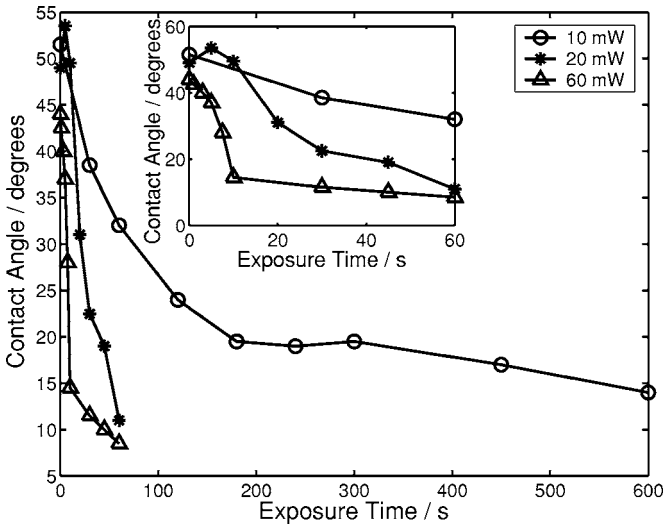

FIG. 2. Change in water contact angle with increasing 244 nm exposure time for powers incident at the chamber of 10, 20, and 60 mW. Inset shows an expanded view of the initial minute. Lines are added to guide the eye.

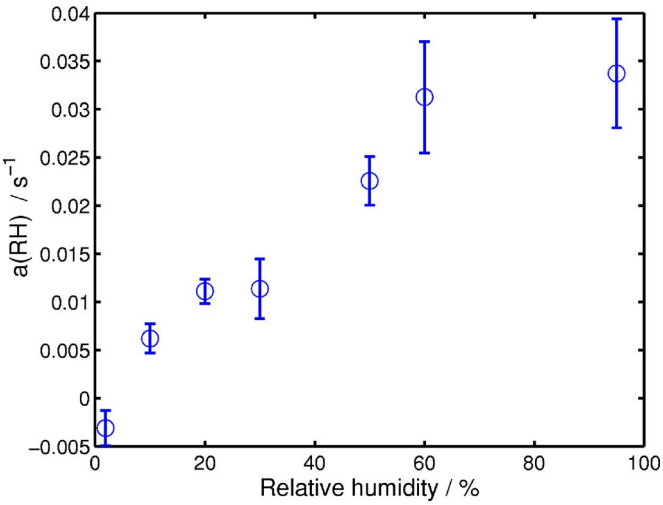

FIG. 3. Change in the parameter a(RH), which describes the strength of the contact angle change, with relative humidity for exposures on the positive z face. Errors are calculated from an error in θ of ±2.8° (P=45 mW).

picture [Fig. 1(b)] shows a drop of the same volume on a preilluminated surface. After sufficient illumination, the contact angle of the drop decreases to a superhydrophilic state ($\theta_E < 5°$) and the surface approaches complete wetting ($\theta_E = 0°$).

All lasers used were seen to produce a change in the hydrophilicity. The $\lambda = 244$ nm laser was chosen for the bulk of the investigation because of the superior quality of its beam profile. Exposures were carried out on both the positive and negative z faces but no significant difference in their behavior was found.

Figure 2 shows the variation of the water contact angle on the positive z face as a function of exposure time with $\lambda = 244$ nm exposure, for powers (measured before the fused silica window of the chamber) of 10 mW (open circle), 20 mW (filled circle), and 60 mW (triangle). The exposures were carried out at a temperature $T = 27$ °C and relative humidity of 55%. It can be seen from the figure that the contact angle change is not a linear function of the total exposure, i.e., the integrated number of photons arriving at the surface, since doubling the incident power does not simply halve the time required to reach a given contact angle. Rather it is seen that the change is a function of both the total exposure and the incident intensity with higher intensities giving a greater change for equivalent exposure.

The contact angle of olive oil was also measured before and after UV exposure; however, the surface was not seen to become oleophillic since no change in the contact angle was seen even after an exposure of 30 mW for 10 min. Prior to application the drop was strongly pulled toward the sample due to the photoinduced surface charging; however, upon contacting the surface no significant change in contact angle was seen.

The atmosphere was observed to have a pronounced effect upon the hydrophilicity change. It was found that when illuminating with the chamber having been evacuated to a pressure of less than 2 mbars, no significant change to the contact angle was seen even for long exposures (15 min) at 45 mW. It was seen particularly that the presence of water during the exposure was important. The relative humidity at constant temperature was lowered within the chamber by purging with dry nitrogen or increased by bubbling air through de-ionized water and measured with a thermohygrometer. The ambient relative humidity in the lab was 38%. The samples were then illuminated under the desired humidity and then returned to atmospheric conditions for the contact angle measurement. As the humidity was increased the change in contact angle was greater for the same exposure. To keep the contact angle large enough to be measureable the exposure time was decresed as the humidity increased. This means that the change in the contact angle needs to be normalized in some way for analysis. Young's equation relates the surface energies at the solid-liquid and solid-vapor interfaces to the contact angle of the three phase system as

$$\gamma_{lv}\cos(\theta_E) = \gamma_{sv} - \gamma_{sl}, \tag{1}$$

where γ is the interfacial energy and the subscripts lv, sv, and sl correspond to the liquid-vapor, solid-vapor, and solid-liquid interfaces, respectively. Since γ_{lv} is a property of the liquid a change in the contact angle will come about only from a change in $(\gamma_{sv} - \gamma_{sl})$. If it can be assumed that the rate of change of this quantity with UV exposure time is constant within our experimental conditions then so too will be $\cos(\theta_E)$ such that

$$\frac{d\cos(\theta_E)}{dt} = a(\mathrm{RH}), \tag{2}$$

where a is dependent upon the relative humidity (RH) and describes the strength of the contact angle change. This leads to

$$a(\mathrm{RH}) = \frac{\cos(\theta_E) - \cos[\theta_E(t=0)]}{t}, \tag{3}$$

where $\theta_E(t=0)$ is the contact angle of unexposed lithium niobate and t is the exposure time. Figure 3 shows the variation of the parameter a(RH) with relative humidity for expo-

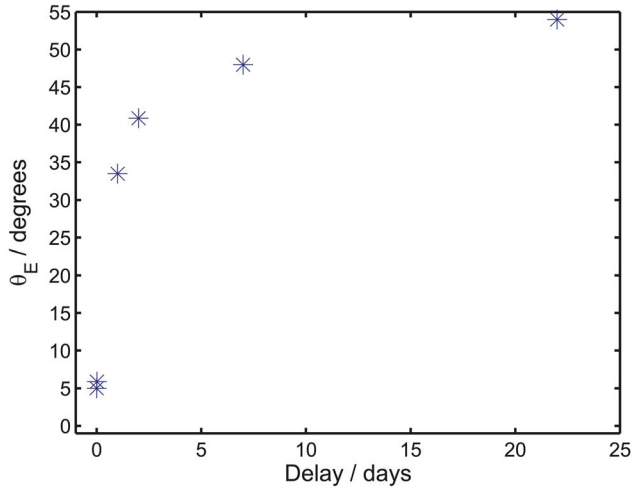

FIG. 4. Recovery of the contact angle with time after exposure of 45 mW for 60 s.

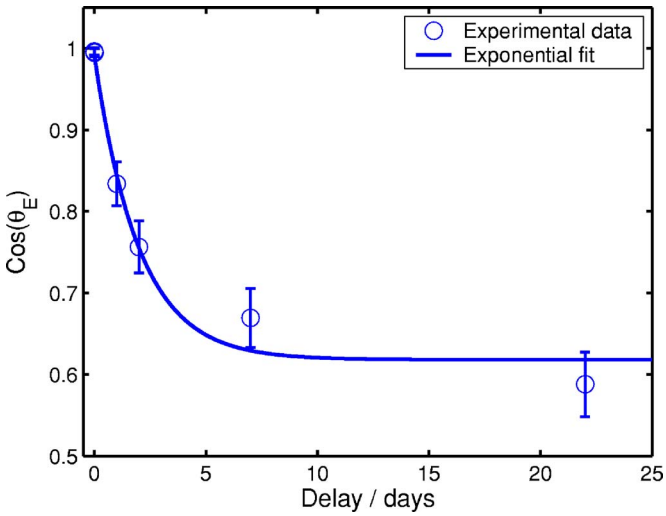

FIG. 5. Decay of the cosine of the contact angle with time after exposure of 45 mW for 60 s. Errors are calculated from an error in θ of ±2.8°.

sures on the positive z face. The error was calculated from the standard deviation (σ) of repeated readings of the contact angle on cleaned unexposed samples, yielding a value of $\sigma = 2.8°$. It can be seen in the figure that there is a linear trend; the change in surface energy being proportional to the number of water molecules present in the atmosphere. The continuation of the trend beyond the ambient humidity, when nitrogen purging was no longer required, indicates that the decrease in UV sensitivity with lowering humidity is indeed due to a reduction in atmospheric water and not due to the displacement of other species by the nitrogen. The value at 95% RH may be reduced due to condensation present upon the sample surface.

In order to study the recovery of the contact angle after exposure a number of samples were exposed at 45 mW for 60 s and then stored individually in polypropelene tubs in the dark. Figure 4 shows that the recovery to the initial contact angle takes around 20 days and that the recovery is not a linear function of time but proceeds at a continuously decreasing rate. If the surface energy change is due to the adsorption of water molecules on the crystal surface, as the humidity dependence suggests, and the thermal desorption of these molecules is a random process with constant probability, then the decay of the surface energy as measured by the cosine of the contact angle should be well modeled by an exponential decay. The decay of the cosine of the contact angle is shown in Fig. 5 with the best fit of the form $y = y_0 + a\exp(-t/\tau)$. The curve fits reasonably well and gives a value of $y_0 = 0.62$ corresponding to a final contact angle of 51.6° which is well within the range of measured unexposed contact angles. The other fit parameters are $a = 0.37$ and $\tau = 2$ days.

From the observed dependence on humidity of the contact angle change after UV exposure it is proposed that the enhanced hydrophilicity is due to dissociative adsorption of atmospheric water onto photoinduced defects creating (hydrophilic) surface hydroxyl groups. The band gap of LN is determined primarily by the properties of the NbO_6 octahedra since the upper level of the valence band is formed by the oxygen electron $2p$ states while the lower level of the conduction band is formed by the d orbitals of the niobium ion.[6] The primary reaction with photons of energy approximately that of the band gap will thus be to create an electron-hole pair bound to a niobium and oxygen ion, respectively. The dissociative adsorption will then proceed as follows:[5]

$$Nb^{5+} + O^{2-} + H_2O \rightarrow Nb^{4+}OH + O^{-}H. \quad (4)$$

The reaction above is similar to that proposed for the UV induced hydrophilicity of TiO_2 (Refs. 7 and 8) and ZnO (Ref. 9) by Watanabe and co-workers. Indeed the band structure of LN is similar to the band structure of TiO_2 since the main building blocks of each crystal are the BO_6 oxygen octahedra with the band gap of TiO_2 being formed by O $2p$ orbitals and Ti $3d$ orbitals and so one may expect the behavior to be similar for $h\nu > E_g$ exposure. This simple hypothesis is, however, shown to be false in Ref. 10, where it is shown that $SrTiO_3$ has no UV induced hydrophilic conversion despite being an ABO_3 oxygen-octahedral dielectric such as LN and having again the similar band structure to both LN and TiO_2. One difference between $SrTiO_3$ and LN, however, is the stacking of the BO_6 octahedra; $SrTiO_3$ is a perovskite-type dielectric that contains corner-sharing oxygen octahedra whereas the LN oxygen octahedra are face sharing. The octahedra in TiO_2 are also face sharing and so this may be another requirement for the hydrophilic conversion process. In Ref. 11, the origin of the UV induced hydrophilic conversion in TiO_2 proposed by Watanabe and coworkers is disputed and attributed solely to the photocatalytic decomposition of organic contaminants which exposes the inherently hydrophilic TiO_2 surface. Although LN also shows a high photocatalytic activity under UV irradiation,[12] our results concerning the humidity dependence of the contact angle change and the fact that no change occurs under vacuum do not support this hypothesis since we see no reason why the photocatalytic decomposition would not occur under these conditions also. In comparison to the hydrophilic conversion in TiO_2 we find that the contact angle change in LN proceeds at a greater rate at the intensities used in this investigation. In Ref. 9, the contact angle change from

the initial angle of 54° to an angle of 10° is seen to take around 5 min for a UV intensity of 50 mW cm^{-2} (λ =365 nm) whereas we see in Fig. 2 that for an exposure of around 20 mW cm^{-2} the change from 55° to 10° is made in just 30 s. In Ref. 11, the change from the initial contact angle (80°) to 15° is seen to take around 18 min for a UV exposure of 13.6 mW cm^{-2} (λ=254 nm) with an initial slope of 4° min^{-1}, whereas in Fig. 2 we see that for an intensity of around 10 mW cm^{-2} the change from 55° to 15° takes around 10 min with an initial slope ($t<200$ s) of around 13° min^{-1}.

Having investigated the behavior of the UV induced hydrophilicity in LN spatial structuring of the surface hydrophilicity, and thus wetting properties was also investigated for possible application in microfluidic devices and sensors.

III. HYDROPHILIC SPATIAL PATTERNING

A. Experimental details

Patterning on the micron scale was achieved by the use of transmission electron microscopy (TEM) hexagonal grids as absorption masks. The grids had hexagonal openings with a diameter of 40 μm (between parallel sides) at a periodicity of 60 μm. The grid was attached to the surface of the sample which was subsequently illuminated under ambient conditions with λ=244 nm light.

Patterning at the submicron scale was achieved either through exposure with an interference pattern of two overlapping beams from the λ=266 nm Nd:YVO_4 laser or by using a phase mask.

Exposures using phase masks were carried out with both the Nd:YVO_4 (λ=266 nm) pulsed source and the λ =244 nm cw source. The phase mask exposures were performed under the same conditions used in the sessile drop experiments. The phase mask used for the λ=244 nm exposures had a period of 1136 nm and the masks used for the λ=266 nm exposures had a period of 1076 nm. The beams used in both cases were divergent and as such the principle modulation of the light intensity pattern at the substrate is expected to be at the phase mask period and not at half of this value as would be expected for a collimated beam.

Visualization of the patterning was achieved through the preferential creation of dew on the exposed areas by cooling the sample in a stream of humid air and visualizing the dew pattern directly using a microscope. The existence of structures was also inferred from diffraction of a He–Ne laser beam from the grating formed by the dew.

B. Results and discussion

Figure 6 shows an optical microscope image of the condensation formed on the $+z$ face after an exposure through the TEM grid (λ=244 nm, 45 mW for 2 min). The sample was cooled by a thermoelectric heat pump to be close to the dew point temperature. The hexagonal lattice which corresponds to the TEM grid pattern can clearly be seen as water vapor from the air preferentially condenses onto the exposed areas. Areas of significant condensation appear darker in the figure while dry areas remain bright. For these exposure conditions the condensation mechanism is seen to be dropwise rather than filmwise.

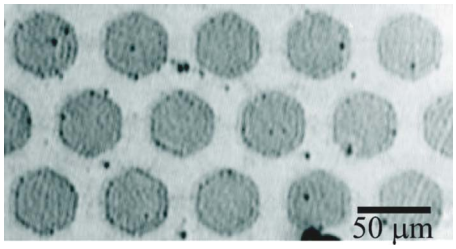

FIG. 6. Condensation pattern formed after cooling in a humid atmosphere. Sample exposed through a TEM grid.

Figure 7(a) shows an optical microscopy image of the preferential condensation of water vapor onto a lithium niobate surface exposed with interfering beams from the Nd:YVO_4 laser. The areas where water is condensing appear dark due to scattering while dry areas appear bright. In this instance it can be seen that the condensation mechanism appears to be filmwise as no discernible drop shapes are present in the condensing areas of the grating pattern. Whether the condensation proceeds as discreet drops or films depends upon the hydrophilicity change that has occurred upon the surface with filmwise condensation occurring for a completely hydrophilic surface (θ_E=0). Since the interfering beams have a Gaussian intensity profile, however, it is possible to view a wide range of illuminating conditions on the same illuminated spot. For example, the microscope image of Fig. 7(b) shows the condensation formed in an area corresponding to lower intensity where the surface does not wet completely and so drops of condensation form. The contrast of the image has been enhanced for clarity and the preferential formation of the drops along the lines of the illuminating interference pattern can be seen clearly.

Diffraction of a He–Ne laser beam (λ=633 nm) was also seen from the submicron structured surfaces due to spatially resolved condensation. The phase mask illuminations create interference patterns with periods of 1136 and 1076 nm for λ=244 nm and λ=266 nm illumination, respectively, giving feature sizes of the hydrophilic patterning of 500 nm. The probe laser beam was incident normally on the sample surface and the diffracted light was measured in transmission. The angles of the m=1 diffracted order in each case were found to be 35.4° for the 1076 nm period mask and 33.9° for the 1136 nm period mask which are within measurement error of the theoretical values of 36.03 ° and 33.9°, respectively.

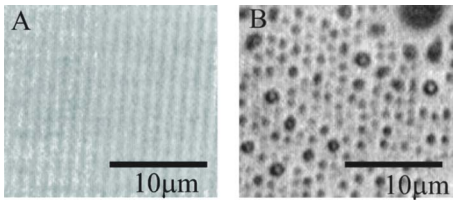

FIG. 7. Condensation patterns formed after an interference pattern exposure: (A) high fluence region with filmwise condensation and (B) low fluence region with dropwise condensation.

We envisage that spatial structuring of the wetting properties with this simple, one step method will enable the creation of microfluidic devices by creating fluid confinement with surface energy barriers, rather than physical barriers such as ridge structures or channels. Since no physical barriers will be present to scatter either optical or acoustic waves, device design can have the flexibility to take full advantage of the many nonlinear optical and acoustic properties for which lithium niobate has become an indispensible material and help create true biological and chemical analysis lab-on-a-chip devices.

IV. CONCLUSION

In conclusion, the hydrophilicity of LN has been seen to undergo a transition from mildly hydrophobic to superhydrophilic under the influence of UV laser light. The hydrophilicity has been shown to be spatially resolvable down to submicron length scale through structuring of the illuminating beam. We propose that the hydrophilic change occurs through the dissociative adsorption of water molecules to form hydrophilic surface hydroxyl groups and this hypothesis has been strengthened by the observation that no change to the hydrophilicity occurs in vacuum and that the hydrophilic change is strongly dependent upon humidity.

ACKNOWLEDGMENT

The authors would like to acknowledge Rutherford Appleton Laboratories Laser Loan Pool for supplying the frequency doubled argon ion laser.

[1] C. L. Sones, S. Mailis, V. Apostolopoulos, I. E. Barry, C. Gawith, P. G. R. Smith, and R. W. Eason, J. Micromech. Microeng. **12**, 53 (2002).
[2] Y. Tomita, M. Sugimoto, and K. Eda, Appl. Phys. Lett. **66**, 1484 (1995).
[3] C. J. Strobl, Z. von Guttenberg, and A. Wixforth, IEEE Trans. Ultrason. Ferroelectr. Freq. Control **51**, 1432 (2004).
[4] Image J: http://rsb.info.nih.gov/ij/; Drop shape analysis plug-in: http://bigwww.epfl.ch/demo/dropanalysis/
[5] M. Maeda, I. Suzuki, and K. Sakiyama, Jpn. J. Appl. Phys., Part 1 **31**, 3229 (1992).
[6] A. M. Prokhorov and Yu. S. Kuz'minov, *Physics And Chemsitry of Crystalline Lithium Niobate* (IOP, Bristol, 1990).
[7] R. Wang, K. Hashimoto, A. Fujishima, M. Chikuni, E. Kojima, A. Kitamura, M. Shimohigoshi, and T. Watanabe, Nature (London) **388**, 431 (1997).
[8] R. Wang, K. Hashimoto, A. Fujishima, M. Chikuni, E. Kojima, A. Kitamura, M. Shimohigoshi, and T. Watanabe, Adv. Mater. (Weinheim, Ger.) **10**, 135 (1998).
[9] R. Sun, A. Nakajima, A. Fujishima, T. Watanabe, and K. Hashimoto, J. Phys. Chem. B **105**, 1984 (2001).
[10] M. Miyauchi, A. Nakajima, A. Fujishima, K. Hashimoto, and T. Watanabe, Chem. Mater. **12**, 3 (2000).
[11] A. Kanta, R. Sedev, and J. Ralston, Langmuir **21**, 2400 (2005).
[12] Z. li, T. Yu, and Z. Zou, Appl. Phys. Lett. **88**, 071917 (2006).